Chapter 6

Hydrodynamics of Ionic Liquids in Bubble Columns

Vicky Lange, Barry J. Azzopardi and Pete Licence

Additional information is available at the end of the chapter

http://dx.doi.org/10.5772/51658

1. Introduction

Over the last ten years, research into ionic liquids (ILs) and their physical/chemical and thermodynamic properties has intensified such that significant progress has been achieved in their application to a wide range of chemical processes. If one considers the patent and secondary literature however, it can be seen that there are very few IL based applications that have successfully reached commercialization. The first IL based process on a pilot scale, called Difasol, was the dimerization of olefins with a biphasic, homogeneous catalyst developed by the Institue Française du Petrole (IFP) [1]. Other examples of applications on pilot scale or even industrial scale include acid scavenging (BASIL, BASF) [2], extractive distillation (BASF) [3], compatibilizers in pigment pastes (Degussa/Evonik) [4], cooling agent (BASF) [5] and storage of gases (Air Products) [6]. It may be a fair assumption that one of the major challenges that restrict their application on an industrial scale is a lack of engineering data which are needed for the optimum scale-up, design and operation of industrial units used with ILs. Thus for the successful transition of ILs from academic labs to industry, not only must the fundamental physical/thermodynamic properties be investigated but we must also better understand the hydrodynamic or flow behaviour that govern reactions on a larger scale under real process conditions. This chapter focuses on IL based multiphase flow, a topic of specific interest to a variety of industrial platforms including biotechnology, biphasic catalysis and gas extraction involving for example H_2, CO, CO_2, H_2S and SO_2.

To apply ILs under multiphasic conditions, the simplest equipment to contact the liquid and gas is the bubble column. In these devices, the gas phase is bubbled through a column of liquid to promote close contact between the two phases. Due to their ease of construction and large applicability, these reactors find widespread use in industry. However despite its simple construction, the hydrodynamics involved inside these units is quite complex because of the very deformable nature of the gas-liquid interface. In bubble column operation, the specific interfacial area is an important criterion since it determines the rate of heat and

mass transfer across the interface. The specific interfacial area is defined as the surface area of the bubbles per unit volume of the reactor space occupied by the two-phase flow mixture. To maximise this area and improve the efficiency of transport processes, small bubbles and a uniform distribution across the column cross section are desired.

This chapter examines how the physical properties of ILs, in particular its viscosity hinder achieving optimally high values of specific interfacial area. Available gas holdup data as well as bubble characteristics are analysed. Firstly factors which can influence the specific interfacial area such as the flow regime and gas holdup are discussed in Section 2. Section 3 describes the experimental approach and measurement techniques employed to study ILs in bubble columns. Bubble formation and coalescence in ILs is examined in Section 4, whilst the effect of operating conditions on the gas holdup is considered in Section 5. Lastly in Section 6, results from statistical analysis of the gas holdup data are presented to describe the frequency and velocity of the flow structures formed.

2. Influencing the specific interfacial area

For a given gas-liquid system, the transport coefficients and the interfacial area are highly dependent on the prevailing operating regime of the bubble column as this is directly related to the bubble size distribution. Because of the very deformable gas/liquid interface, there are a large number of ways in which the different phases may distribute in the column. To simplify this problem, the flow is conventionally distinguished by two main flow regimes, i.e., the homogeneous bubble regime and the heterogeneous (churn-turbulent) regime. The homogeneous regime normally exists at very low gas flow rates and is characterised by smaller, more uniformly sized bubbles which rise with similar velocity. At higher gas flow rates, a wide distribution of bubble sizes is observed due to bubble coalescence and the flow is described as heterogeneous. In this regime, the bubble swarm consists mostly of large fast-ascending bubbles and a few smaller bubbles which are trapped in the liquid recirculation flow. In cases where the column diameter is small (≤100 mm), the larger bubbles of heterogeneous flow are stabilised by the surrounding walls and can occupy the entire column cross section, forming gas plugs (called slug flow). As a result of the larger, fast-ascending bubbles, the mean gas phase residence time and the specific interfacial area in the heterogeneous regime is lower in comparison to the homogeneous regime. In reality, due to high gas throughputs the heterogeneous regime is often observed in industrial bubble columns. Although, the homogeneous regime which offers greater interfacial contacting and a low gas shear environment can be more desirable, in particular for those applications which involve sensitive media, for example biotechnology.

To estimate the specific interfacial area, the bubble size distribution is used in conjunction with the gas holdup or void fraction. The gas holdup is defined as the fraction of the gas present in the two-phase mixture in the reactor. It depends strongly on the operating conditions, physiochemical properties of the two phases, the gas distributor design (the number and size of the holes) and the column geometry (height to diameter ratio). To better under-

stand the effect of these parameters on the flow behaviour in the bubble column, their effect on the gas holdup and the gas flow rate has been investigated by several researchers through extensive experimentation as well as theoretical analysis in the last few decades. An extensive review was given by [7], and there have been continuous publications since.

Understanding the effect of system pressure (or gas density) has been important since most industrial applications of bubble columns operate under pressurized conditions. This is because the increased solubility of a gas with pressure is expected to enhance the mass transfer and reaction rates. Based on the findings by several workers [8-15], it has been commonly established that gas holdup increases with operating pressure. The increase of gas holdup at the elevated system pressures has been attributed to the smaller bubbler size which is caused by a reduction in the coalescence rate, the enhancement of the bubble breakup or the decreased size of bubbles formed at the gas disperser [16-18].

The effect of the liquid phase properties has also been investigated, although to a lesser degree. For convenience, most studies of bubble columns have used water as the liquid phase, even though in reality the physical properties of many of the liquids used industrially differ significantly from those of water. In particular, the ILs considered here have viscosities considerably higher than water. Several studies have looked at the effect of liquid viscosity during bubble column operation [19-26]. These show that at a given gas flow rate, the gas holdup decreases with increasing viscosity. Furthermore in a larger diameter column, the transition point from homogeneous to heterogeneous flow has been found to shift to lower gas velocities with increasing liquid viscosity.

3. Determination of gas holdup

When a gas is bubbled through a column filled with liquid, the bed of liquid begins to expand or swell as soon as gas is introduced. If the gas holdup is expressed in terms of a global or total voidage for a bubble column, it can be calculated by measuring the difference between the gassed and ungassed height of the liquid since this represents the total gas volume present in the column. The total gas holdup can also be determined from pressure gradient measurements using pressure sensors. However, in cases where more local information on the gas phase is required, the gas holdup can be measured by a selection of invasive or non-invasive techniques. A comprehensive review of methods which can be applied for closed systems (pipes, columns etc.) was presented in [27], wherein all pertinent literature until roughly 1977 was surveyed. More recent reviews have been presented by workers such as [28] and [29]. Examples of some of the options available include using needle probes, quick-closing valves (QCVs), flush mounted conductance probes, capacitance probes, wire mesh sensors, neutron and radioactive absorption, resistive and ultrasonic tomography.

To obtain the local gas holdup for an IL, the conductance probe is an appropriate choice since the IL is a very good electrical conductor, while the conductivity of the gas phase is infinitely low. This measurement technique follows the approach developed by researchers such as [30], whereby the electrical impedance of the gas-liquid region close to a system of

electrodes is measured and the phases distinguished due to the difference in the electrical conductivity of the phases. The conductivity is measured between two metallic rings (ring-type conductance probe) which are mounted flush with the bubble column walls. For the experiments presented here, the metallic rings were constructed by placing two stainless steel plates between three alternating plates of an acrylic resin and machining out a cylinder through them which had an internal diameter equal to the column diameter. Figure 1(a) shows a picture of these probes, while a schematic of their configuration is presented in Figure 1(b). The configuration is characterised by the thickness of the rings s and the spacing between them D_e. The column diameter is represented by D_t. The dimensions D_e/D_t and s/D_t were 0.357and 0.075 respectively.

Each probe pair was supplied with an a.c. carrier voltage of -1 to 1 volt peak to peak, at a frequency of 20 kHz. An instrumentation amplifier, a full wave rectifier and a band pass filter were installed before the signal was sent to the data acquisition board. A cut-off frequency of 100 Hz was applied in order to eliminate the high frequency noise generated from the power supply. To account for any differences in the test fluid conductivity during experiments due to any temperature variations, all conductivities were normalized to produce a dimensionless conductance by measuring the conductivity at the start of each experimental run with the column full of liquid.

To obtain values for gas holdup from the conductance measurements, it is necessary to determine the relationship between the liquid phase conductance and gas holdup. This relationship is obtained via careful calibration. The simplest approach involves artificially creating instantaneous gas fractions between the probes, for example using plastic non-conducting beads to simulate bubbly flow inside the column. A detailed description for the calibration procedure is available in [31].

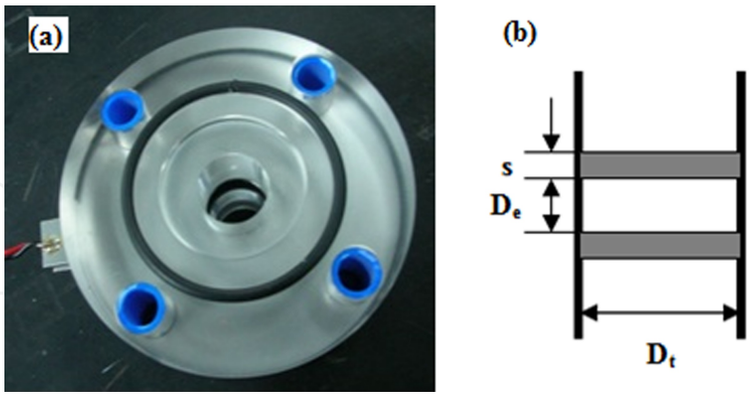

Figure 1. Conductance Probe: (a) picture; (b) schematic of ring shaped conductance probe.

For the IL 1-ethyl-3-methylimidazolium ethylsulfate, $[C_2C_1Im][EtOSO_3]$, the time-varying gas holdup in a cylindrical bubble column (inner diameter 0.038 m; height 1.1 m) has been measured by utilising two pairs of conductance probes installed flush in the column walls. The experimental setup is illustrated in Figure 2. For comparison, water, a glycerol/water solution and solution of glycerol/water with sodium chloride dissolved in it were also inves-

http://dx.doi.org/10.5772/51658

tigated. To prepare the glycerol solutions, a total of 15% of weight of water was mixed with glycerol to produce a liquid which has a viscosity similar to that of $[C_2C_1Im][EtOSO_3]$. A total of 1.3% by weight of sodium chloride was also added to one of the glycerol/water mixtures to ensure sufficient conductivity for use with the conductance probes. The physical properties of the liquid phases used in all experiments at 20°C are summarised in Table 1. To determine the viscosities and conductivities of the liquids a Brookfield viscometer and WTW KF 340 conductivity meter were used respectively. The viscosity of water and surface tensions were obtained from physical property tables. The properties of $[C_2C_1Im][EtOSO_3]$ were obtained from the paper by [32].

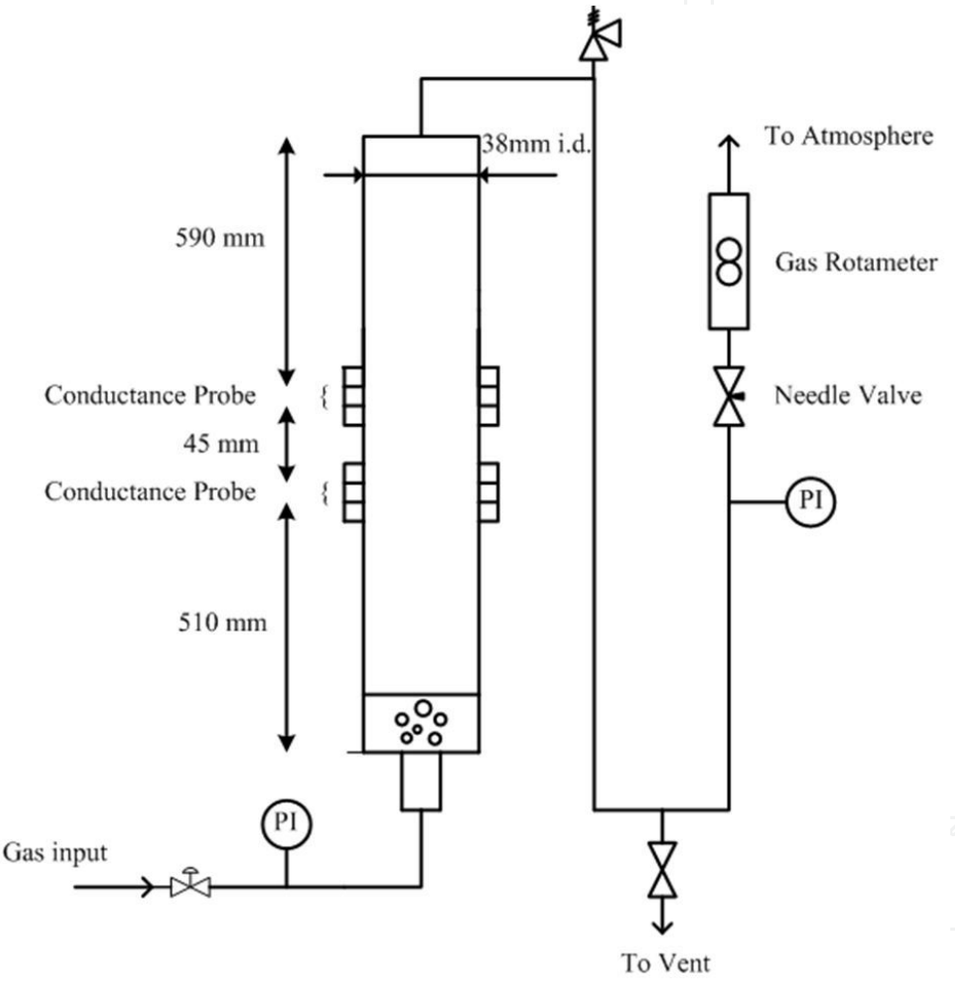

Figure 2. Experiment setup for gas holdup measurements.

Prior to experiments, $[C_2C_1Im][EtOSO_3]$ was dried and degassed under vacuum at 60°C for 24 hours since it is known that ILs will absorb a couple weight percent of water when left open to the atmosphere. Here, the main concern is the effect of the absorbed water on the physical properties of $[C_2C_1Im][EtOSO_3]$, in particular its viscosity as well as ion mobility which relates to its electrical conductivity. The estimated water content of $[C_2C_1Im][EtOSO_3]$ after drying was approximately 0.76 wt% water, as measured by Karl Fischer test.

Property	$[C_2C_1Im][EtOSO_3]$	Glycerol (15% water)	Glycerol (15% water + 1.3% NaCl)	Water
Density (kg/m^3)	1241	1212	1224	1000
Viscosity (mPa s)	91.5	93.1	107.9	1.09
Surface tension (N/m)	0.047	0.062	0.062	0.072
Conductance (S/cm)	4160	1.4	485	42

Table 1. Physical properties of the liquid phases (T = 20˚C).

Measurements for gas holdup at a given operating pressure were performed by increasing the gas superficial velocity to a maximum value of 60 mm/s, while the operating pressure was systematically varied in the range of 0.1-0.8 MPa. The column was first filled with the liquid under test at room temperature (20˚C) and compressed nitrogen gas from a gas cylinder was then fed into the bottom of the column through a single nozzle gas distributor which had an inner diameter of 0.635 mm. Glass beads were also employed at the gas inlet to the column for improved phase distribution. A pressure regulating valve at the gas cylinder fixed the maximum gas inlet pressure and a pressure relief valve set at 15 MPa protected the facility against overpressure. Flow was created in the system by using a needle valve which was installed at the inlet to a gas rotameter and had an outlet open to the atmosphere. To minimise liquid carry-over from the column into the downstream instrumentation, several pieces of wire mesh were installed at the top of the column to catch stray droplets.

4. Bubble Formation and Coalescence

When a gas is passed through an orifice into a pool of liquid, certain forces act on the gas which breaks it up to form individual bubbles. If the bubble column is transparent, photographic techniques involving a high-speed camera can be quite helpful to analyse the shape and the size of the bubbles formed. Stills taken from high-speed videos at atmospheric pressure of $[C_2C_1Im][EtOSO_3]$, glycerol solutions and water are shown in Figure 3. These reveal that even at the lowest gas superficial velocity (u_{gs} = 3 mm/s), the homogeneous flow regime is essentially absent for the IL and the glycerol solutions. In a distinct contrast to water, it is seen that the bubbles formed in these high viscous liquids are bigger and less uniform in size.

In $[C_2C_1Im][EtOSO_3]$ three different sized bubbles are formed. The largest are bullet-shaped Taylor bubbles which characterize slug flow. These only occur for the largest gas flow rates studied; instead clearly defined spherical-cap shaped bubbles are formed at velocities ≥ 15 mm/s. The second, intermediate sized bubbles in the IL are essentially spherical of 0.5 – 2.5 mm, while the smallest are also spherical however with diameters ≤ 250 μm. It is believed that the smallest bubbles are formed by the bursting of Taylor bubbles at the gas/liquid interface. These tiny bubbles formed have very low rise velocities and tend to flow with the liquid. As a result, they can be distributed throughout the entire column due to backmixing of the liquid.

http://dx.doi.org/10.5772/51658

As the bubbles rise in the column, their size can decrease or increase through various breakup or coalesce mechanisms respectively. In both $[C_2C_1Im][EtOSO_3]$ and glycerol solutions coalescence is observed immediately at the lower gas velocities. In contrast, due to the reduced viscosity in water coalescence is only seen at velocities > 30 mm/s. The smaller viscous or drag forces in water also leads to the formation of spherical-cap bubbles which in comparison to the IL and other viscous liquids, are rather irregular and distorted in shape (Figure 3(D)).

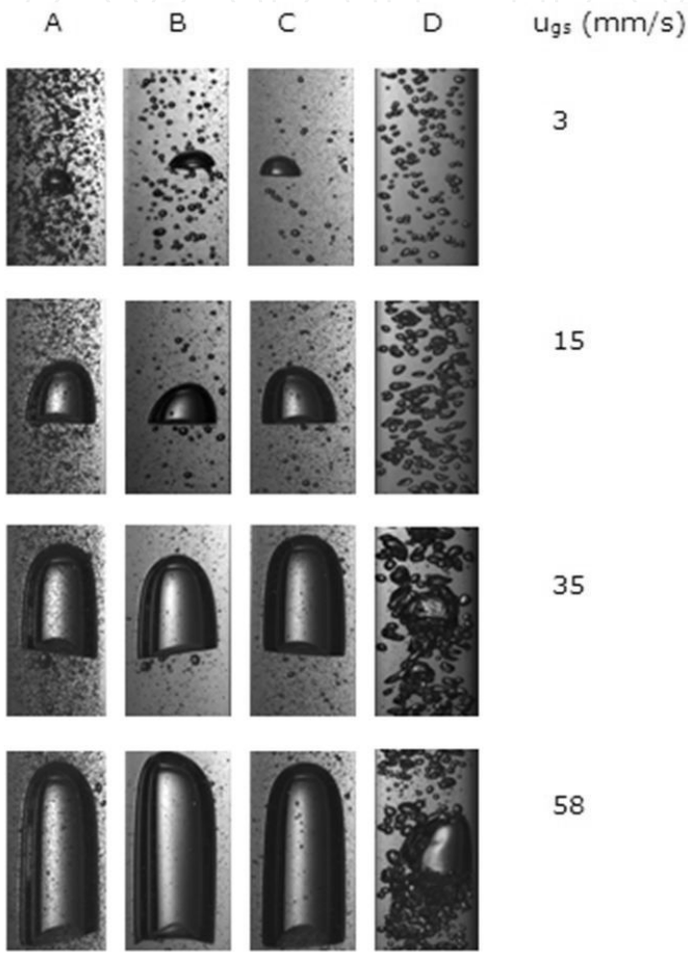

Figure 3. Stills taken from high-speed videos illustrating typical flow structures. The letters identify the liquids (A) $[C_2C_1Im][EtOSO_3]$; (B) glycerol (15% water); (C) glycerol (15% water + 1.3% NaCl); (D) water.

In the IL, coalescence of Taylor or spherical-cap bubbles is frequently observed, however coalescence between spherical-cap and intermediate bubbles is less common. In Figure 4, the coalescence between two spherical-cap bubbles is shown as an example. In the first frame the lower bubble appears to be distorted by being in the wake of the upper spherical-cap bubble. It can also be seen that the intermediate-sized bubbles in the wake of the leading spherical-cap bubble do not coalescence with the upper bubble but instead they are forced to one side by the arrival of the second spherical-cap bubble. Thereafter the intermediate-sized bubbles eventually reposition themselves in the wake of the combined spherical-cap bubble.

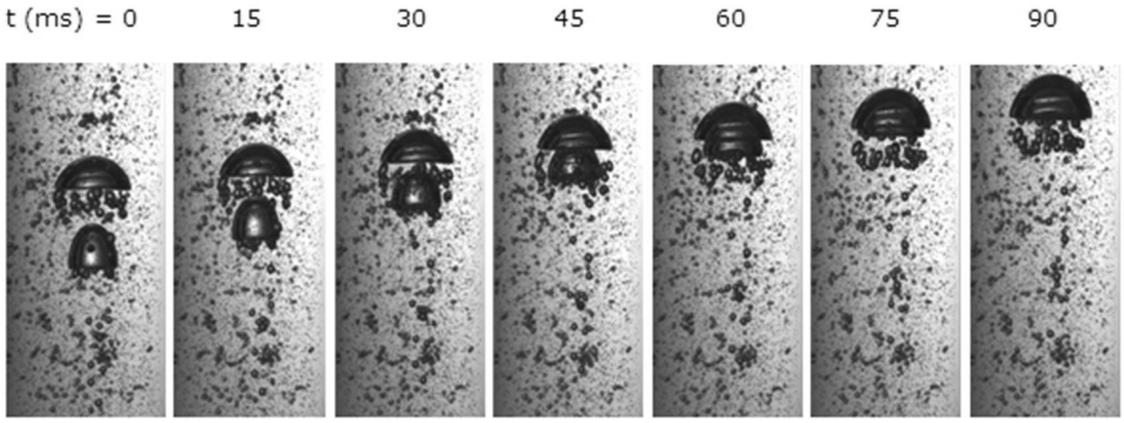

Figure 4. Sequence of stills from high-speed videos illustrating the coalescence of two spherical-cap bubbles in $[C_2C_1Im][EtOSO_3]$.

Bubble coalescence in $[C_2C_1Im][EtOSO_3]$ was also observed in high-speed videos taken of a larger diameter column (125 mm) with a gas distributor consisting of a plate with 25, 1 mm diameter holes. Trailing bubbles were seen to travel considerable distances across the column, move into the wake of a preceding one and then coalescence. A still at a gas superficial velocity of 10 mm/s is provided in Figure 5, which shows the formation of small spherical-cap bubbles even in the larger sized column.

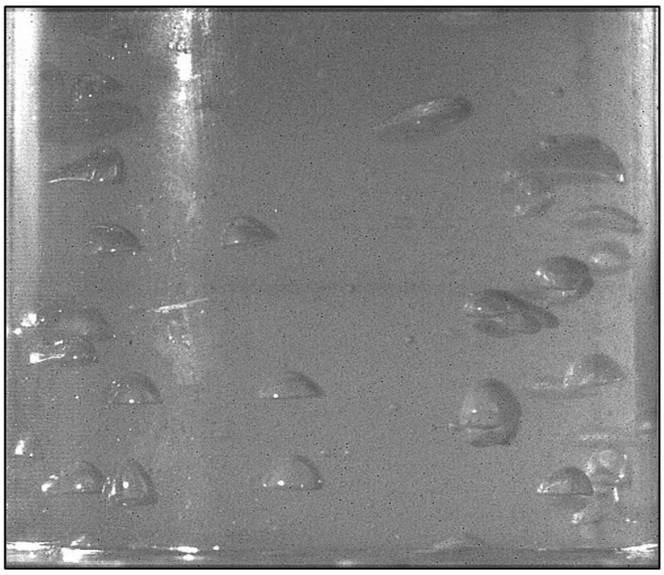

Figure 5. Still from high-speed video illustrating the formation of spherical-cap bubbles in 125 mm i.d. column filled with $[C_2C_1Im][EtOSO_3]$. (taken by D. Sreevasan)

The behaviour of single bubbles rising through liquids has been classified on the basis of three dimensionless groups, Morton, Eötvös and Reynolds numbers, defined as $\mu^4 g\Delta\rho/\varrho^2\sigma^3$, $g\Delta\rho D^2/\sigma^3$ and $\rho uD/\mu$ respectively. Here μ is the liquid viscosity, g the acceleration due to gravity, $\Delta\rho$ is the difference between the gas and the liquid, ρ is the liquid density, σ is the surface tension,

D is the column diameter and *u* is its rise velocity. The ranges of the dimensionless groups for which different types of bubbles exist and in which the effects of the channel walls become important has been identified by [33]. For $[C_2C_1Im][EtOSO_3]$ the Morton number is 0.014 and the Eötvös number on the order of 400. It is found that the characterization map of [33] accurately predicts the formation of spherical-cap bubbles at smaller bubble sizes.

The motion and deformation of a single bubble rising in ILs ($[C_4C_1Im][BF_4]$, $[C_8C_1Im][BF_4]$and $[C_4C_1Im][PF_6]$) were also studied by [34] through image analysis of high-speed videos. Two new empirical correlations were proposed to correlate the drag coefficient as a function of Reynolds number and the aspect ratio as a function of a new dimensionless parameter which could group experimental data for bubbles in ILs. The predicted drag coefficients agreed well with the experimental data however, further experiments are needed to verify these new correlations for a wider range of ILs with different ion pairs and physical properties.

5. Gas holdup at low and elevated pressures

To achieve a better understanding of the flow phenomenon present time traces of the gas holdup obtained from the conductance signals can be analysed by using statistical functions. Time-averaged values are usually obtained first and thereafter, the variations in the amplitude and in the frequency space can be explored. In each experiment presented here, the gas holdup was measured by sampling the data at 1000 Hz over a time period of 60 s. Examples of time traces at the same gas superficial velocity (u_{gs} = 50 mm/s) are given in Figure 6. Figure 6(a) shows the effect of increasing pressure in the IL system. At 0.1 MPa, the time series shows periods of very low gas holdup values which alternate with significant periodic increases to the gas holdup. This confirms the presence of alternating aerated liquid slugs with large gas pockets and even Taylor bubbles which were seen in the photographs. In contrast, at 0.8 MPa the time trace shows that the flow is no longer intermittent. The peaks are noticeably lower and non-uniform which indicates a bubbly heterogeneous flow of smaller sized bubbles.

In Figure 6(b), it is seen that similar time traces are obtained for $[C_2C_1Im][EtOSO_3]$ and the glycerol solutions at 0.8 MPa suggesting that similar sized bubbles were present in both viscous systems. However when compared with water at 0.8 MPa (Figure 6(c)) a more uniform time trace of smaller gas holdup values is observed for water which suggests that the 'larger' bubbles present in the heterogeneous flow in the viscous systems did not form in water.

Time-averaged gas holdup values have also been calculated and plotted against gas superficial velocity for the liquids. Figures 7(a) and 7(b) show examples at atmospheric pressure and at a pressure typical of industrial conditions (0.8 MPa) respectively. These increase monotonically with gas superficial velocity. In comparison to water, the gas holdup in $[C_2C_1Im][EtOSO_3]$ is significantly lower while similar results are obtained for $[C_2C_1Im][EtOSO_3]$ and the viscous glycerol solutions. It is therefore reasonable to conclude that the observed reduction in the gas holdup in $[C_2C_1Im][EtOSO_3]$ is due to its higher viscosity. For high viscous media in bubble columns, the reduced gas holdup can be attributed to increases in the magnitude of viscous or drag forces exerted during bubble formation so that a stable bubble di-

ameter is attained before its detachment at the gas distributor. By stabilizing the bubble interface, bubble coalescence is promoted and bubble breakup is suppressed in the gas distributor region. It is probable that this led to the formation of larger fast-rising bubbles in the IL and glycerol solutions. These faster bubbles spend a shorter time in the column and consequently the overall gas holdup is decreased.

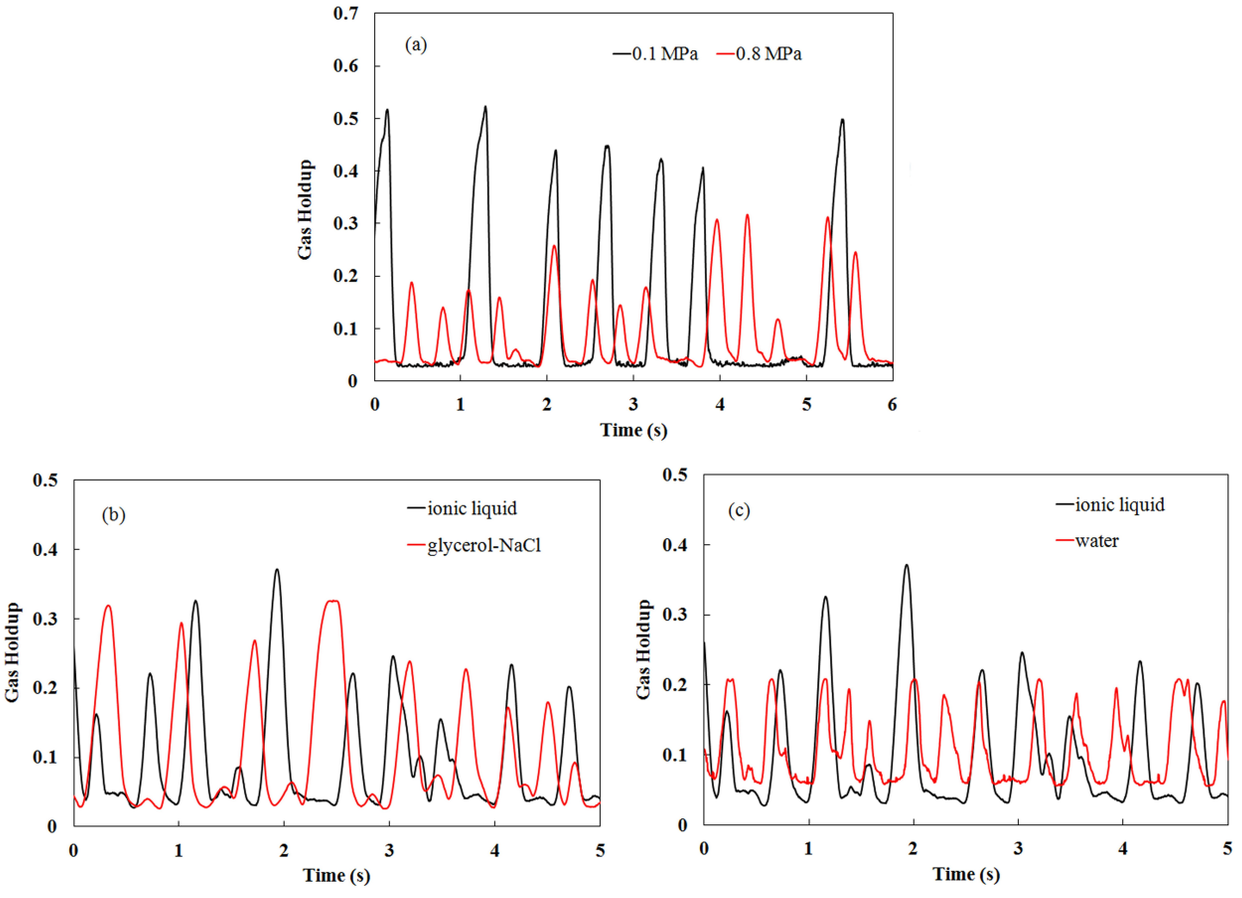

Figure 6. Gas holdup time trace: (a) $[C_2C_1Im][EtOSO_3]$ at 0.1 and 0.8 MPa; (b) $[C_2C_1Im][EtOSO_3]$ and glycerol-NaCl; (c) $[emim]EtSO_4$ and water.

For the estimation of the gas holdup, there exists a vast number of equations in the open literature, most of which are empirically based. In the review by [35], 37 published equations for gas holdup are listed. In selecting equations to predict gas holdup overall correlations based on experimental data is often used, despite the fact that it is generally better to use more physically based methods since empirical correlations are usually most suited for the experimental conditions which they were developed from. However, due to the extreme sensitivity of the gas holdup to other factors for example the gas distributor design, purity of the continuous phase and the physical properties of the phases, developing a generalised model can be complex.

The time-averaged gas holdup data for $[C_2C_1Im][EtOSO_3]$ was tested against three available models in the literature: Urseanu et al. [26], Wilkinson et al. [20] and Krishna et al.

http://dx.doi.org/10.5772/51658

[36]. It was found that the prediction by [26] gives the best agreement at both low and elevated pressures (Figure 8). This model was based on their work with high viscous liquids (0.05-0.55 Pa s) at elevated pressures (0.1-1 MPa). The model by [20] which was developed specifically for the industrial scale-up of pressurized bubble column reactors is presented in Figure 9. The model is shown to be reliable at lower gas superficial velocities while the correlation by [36] significantly overestimates the gas holdup in the homogenous regime as well as the transition point.

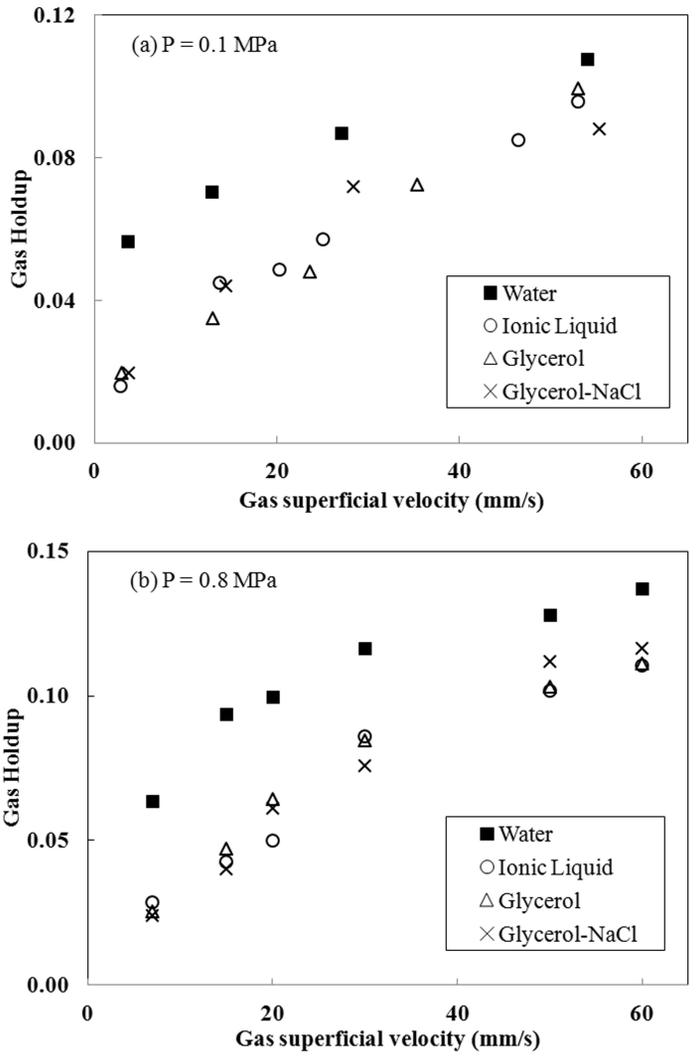

Figure 7. Effect of liquid viscosity on the average gas holdup: (a) P = 0.1 MPa; (b) P = 0.8 MPa.

The effect of system pressure (or gas density) on the gas holdup can be significant in certain circumstances. Figure 10 shows how increasing the pressure increases the time-averaged gas holdup in $[C_2C_1Im][EtOSO_3]$, water and glycerol solutions. It is believed that increased system pressure leads to enhanced local turbulence. This destabilises the larger bubbles that would otherwise form in the heterogeneous regime at atmospheric pressure. As a result bubble breakup occurs and small bubbles which have lower rise velocities are created. These bubbles have

longer residence times in the column and the gas holdup is consequently increased. However it is clear that for the range of gas superficial velocities investigated, the change in gas holdup with pressure is not very significant for $[C_2C_1Im][EtOSO_3]$. Similar findings were reported by [26] in their work with high viscous oils at elevated system pressures.

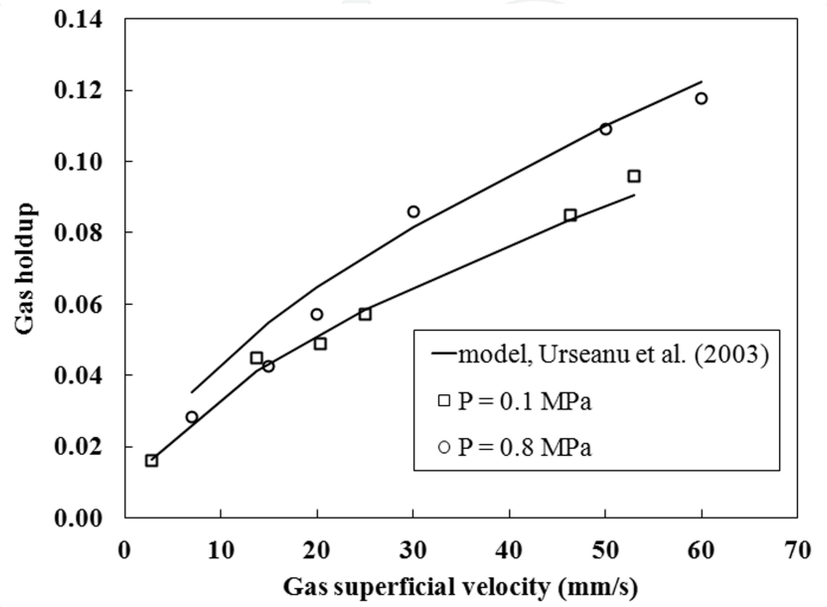

Figure 8. Comparison of predictions of the correlations of Urseanu et al. [26] with the present gas holdup data for $[C_2C_1Im][EtOSO_3]$.

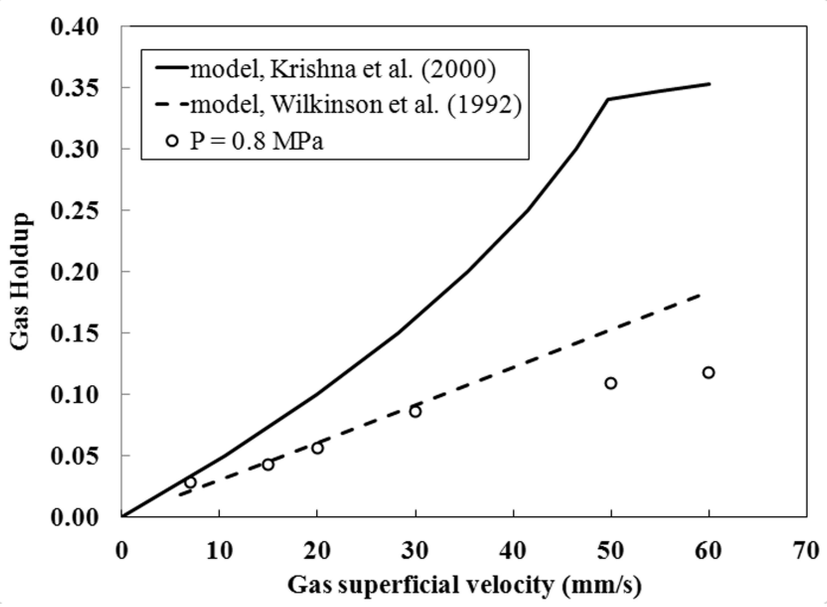

Figure 9. Comparison of predictions of the correlations of Krishna et al. [36] and Wilkinson et al. [20] with the present gas holdup data for $[C_2C_1Im][EtOSO_3]$.

http://dx.doi.org/10.5772/51658

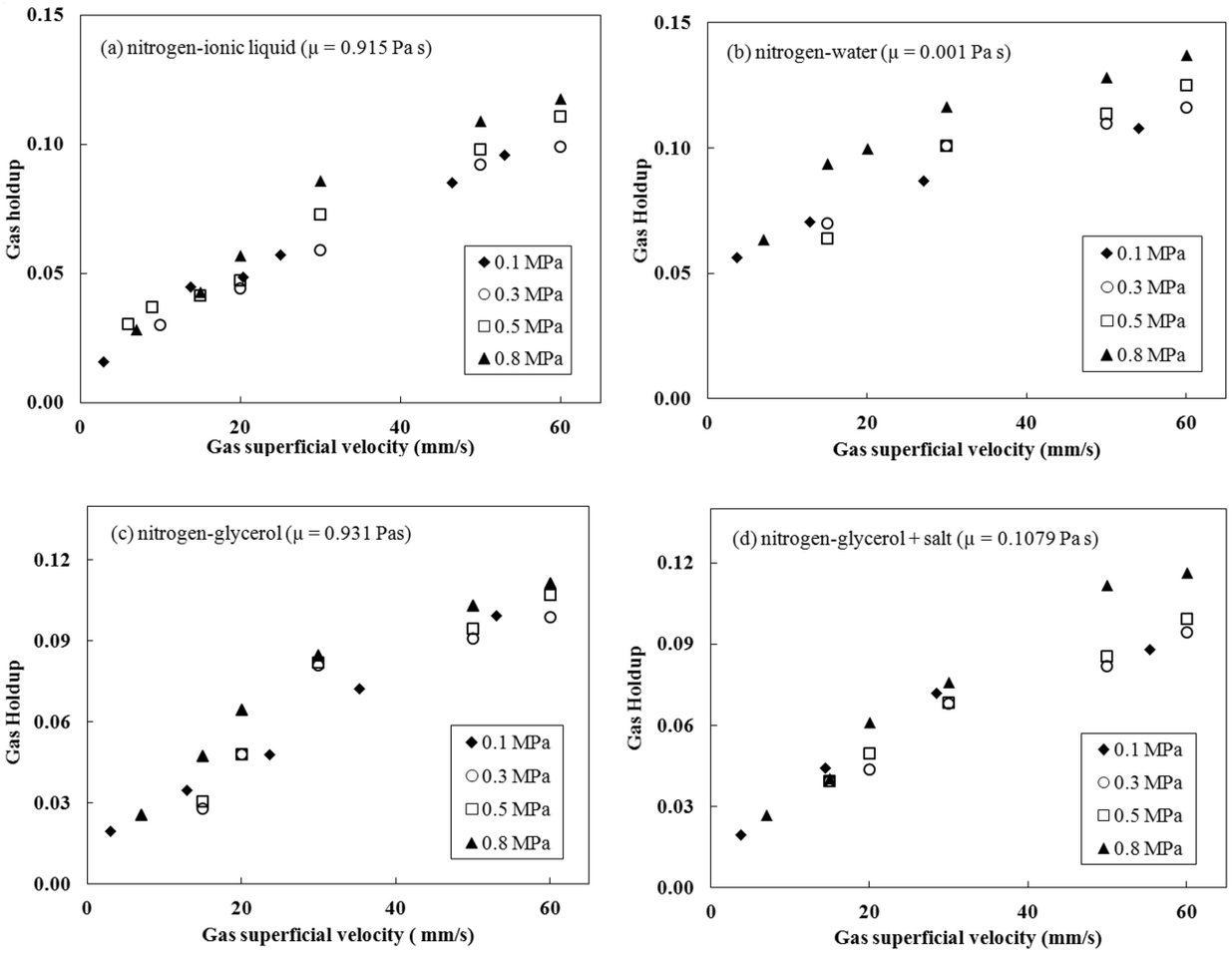

Figure 10. Effect of system pressure on gas holdup: (a) $[C_2C_1Im][EtOSO_3]$; (b) water; (c) glycerol; (d) glycerol + 1.3% NaCl.

6. Detailed Behaviour of the Flow

6.1. Flow patterns

To examine the flow in more detail, the variations in amplitude of the gas holdup time traces can be considered using the probability density functions (PDFs), i.e., the fraction or how often particular gas holdup values occur. In the approach made popular by [37], PDF plots of gas holdup time series are often used to identify different flow patterns in gas-liquid flows, based on the distinctive shape that exists for each regime. For example, the signature PDF for homogeneous bubbly flow is characterised by a narrow single peak at low gas holdup, whereas the PDF for slug flow is double-peaked. PDFs for $[C_2C_1Im][EtOSO_3]$ and glycerol are presented in Figures 11 and 12 respectively. It is seen that the shapes of the PDFs for both liquids are quite similar. At atmospheric pressure, there is a single peak at low gas holdup with a broadening tail which extends to a smaller second peak at higher gas holdup values. According to [37] this signature shape is indicative of spherical-cap bubbly flow or

even slug flow. The small second peak for the spherical-cap bubble is marked with arrows. This is validated by what was seen in the high-speed videos (Section 3).

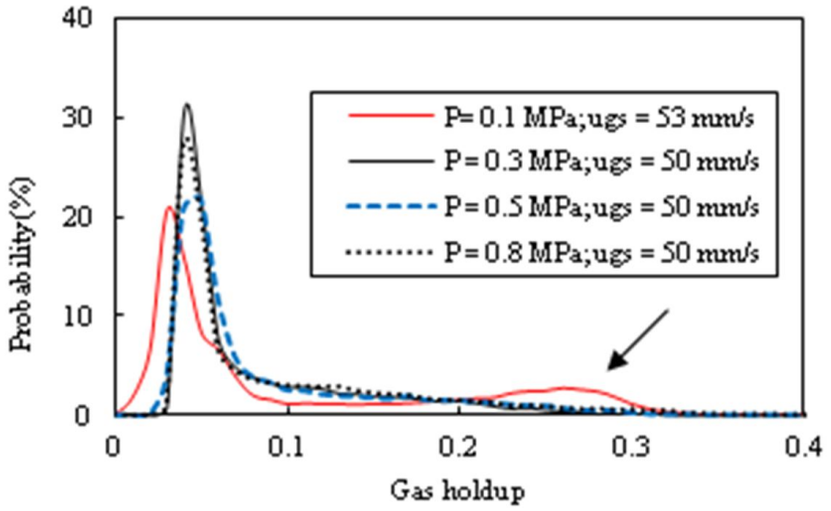

Figure 11. PDF of gas holdup: $[C_2C_1Im][EtOSO_3]$.

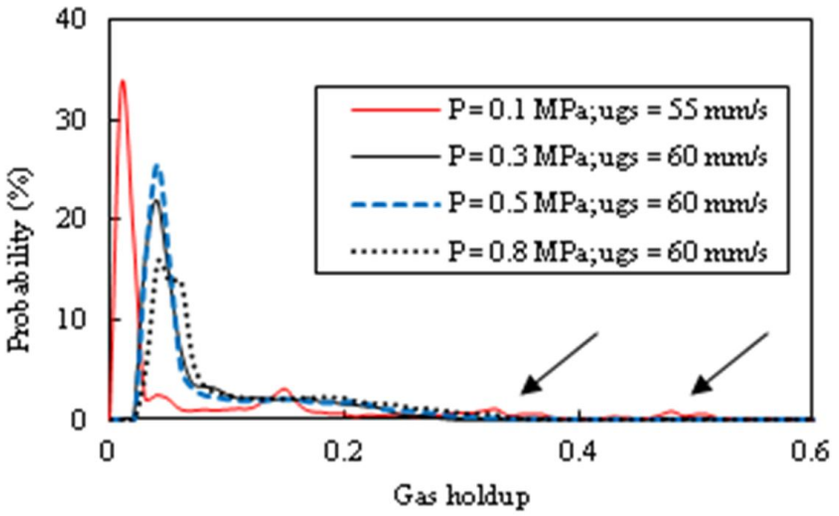

Figure 12. PDF of gas holdup: glycerol.

At higher pressures, the probabilities of higher gas holdup values decrease for both $[C_2C_1Im][EtOSO_3]$ and glycerol. This provides evidence that Taylor or larger spherical-cap bubbles are not formed in the viscous systems at system pressures exceeding atmospheric. Instead the PDF traces are single-peaked, although there is some spread in the distributions which suggests that the flow consists of unequally sized bubbles, i.e., heterogeneous. The Morton number and the Eötvös number for $[C_2C_1Im][EtOSO_3]$ were on the order of 50 and 30 respectively for the system at higher pressures. The characterization map of [33] predicts that ellipsoidal bubbles instead of spherical-cap bubbles are expected. It also indicates that the terminal velocities of the bubbles will be strongly influenced by the walls.

http://dx.doi.org/10.5772/51658

Generally for gas-liquid flows, the most common way of identifying which flow pattern occurs for a given set of flow rates is to use a flow pattern map. For bubble columns, these flow pattern maps are often plots of the gas superficial velocity against the column diameter. If the gas holdup data for $[C_2C_1Im][EtOSO_3]$ is plotted on such a graph, conditions at which heterogeneous flow were observed would be in the homogenous region of the map. The inability of these maps to accurately predict the flow regimes in high viscous media such as $[C_2C_1Im][EtOSO_3]$ is probably due to the fact that they have been developed empirically using data obtained from air-water experiments.

6.2. Structure frequencies

Much can also be learned about the flow structures in $[C_2C_1Im][EtOSO_3]$ by examining their frequencies. This can be obtained by power spectrum analysis of the gas holdup time traces. Here, power spectrum densities (PSDs) have been obtained by using the Fourier transform of the auto-covariance functions. Essentially the Fourier transform is used to transform the time series from a time domain into a frequency spectrum. Examples of PSDs for $[C_2C_1Im][EtOSO_3]$ at 0.8 MPa are shown in Figure 13. At each gas flow rate, a clear peak in the range of 2 – 2.5 Hz is seen. These peak values are the frequencies of recurrence of any periodic structures. The frequencies obtained using this method have been compared with those determined from manually counting the peaks in the time traces. Values obtained from the two methods agree within 10%.

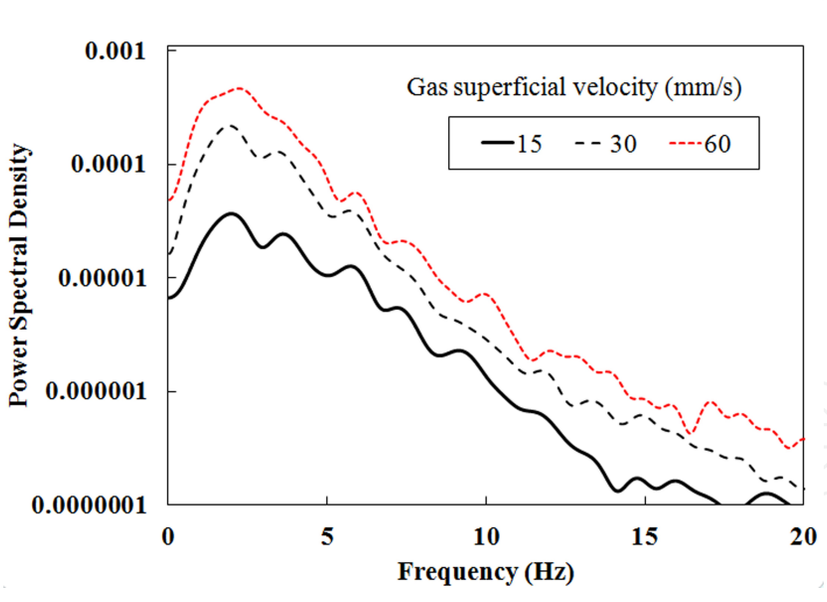

Figure 13. PSD of gas hold time series: liquid = $[C_2C_1Im][EtOSO_3]$.

The effect of increasing pressure on the structure frequencies in $[C_2C_1Im][EtOSO_3]$ is shown in Figure 14. It is seen that for the same gas flow rates, the frequencies generally increase with increasing system pressure. The increasing number of structures at higher pressures further suggests that at higher pressures bubble breakup or coalescence suppression occurs in $[C_2C_1Im][EtOSO_3]$.

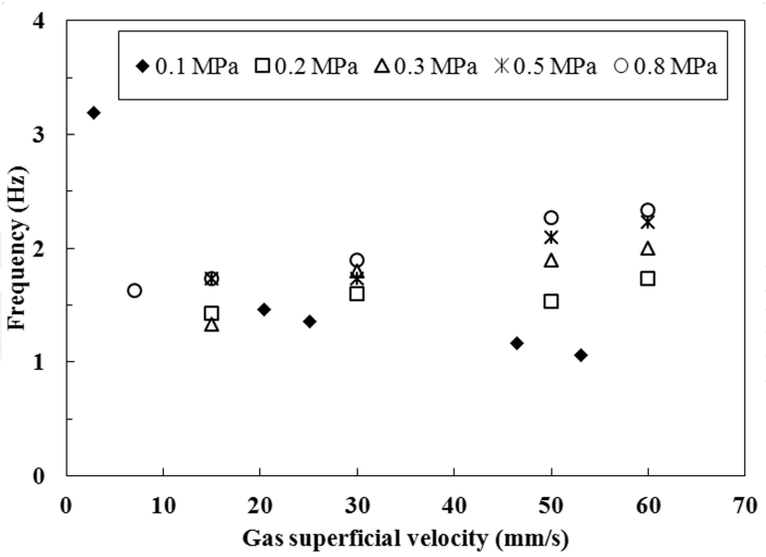

Figure 14. Effect of system pressure on the structure frequencies in $[C_2C_1Im][EtOSO_3]$.

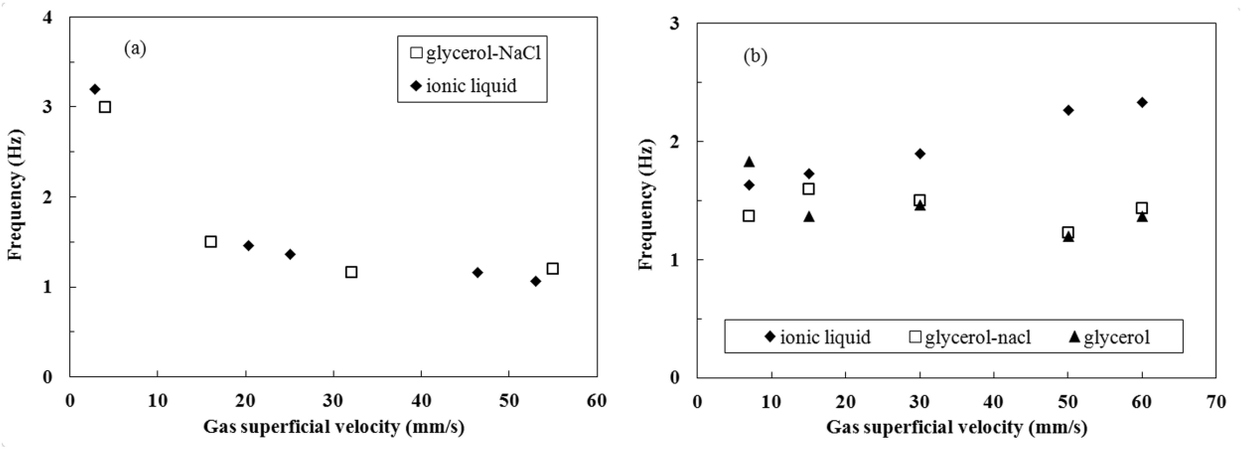

Figure 15. Effect of the liquid on the frequency: (a) 0.1 MPa; (a) 0.8 MPa.

The frequencies obtained for $[C_2C_1Im][EtOSO_3]$ at 0.1 MPa and 0.8 MPa can also be compared to the equivalent data for glycerol-NaCl. These are shown in the subplots presented in Figure 15. At atmospheric pressure it is seen that there are only small differences between the frequencies for the different liquids and they decrease with increasing gas flow rates. However at a higher system pressure, larger variation is observed particularly at the highest gas flow rates. To analyse this further aspects of the axial variations in the flow have also been examined. The flow development in $[C_2C_1Im][EtOSO_3]$ and glycerol-NaCl based on their frequency and PDF data obtained from both conductance probes are shown in Figures 16 and 17 respectively. It is seen that frequencies obtained for the probe downstream (B) in $[C_2C_1Im][EtOSO_3]$ is slightly higher than probe upstream (A) while the PDF downstream displays a taller peak indicating a larger probability of small gas holdup values there. The opposite is observed in the results for glycerol-NaCl. A possible explanation for this could

be that the difference in molarity between the two liquids had an effect on the coalescence of bubbles. The glycerol-NaCl solution has a molarity of 0.17 M, while that of $[C_2C_1Im][EtOSO_3]$ is essentially infinite. In the literature, a critical value of 0.2 M has been cited for the suppression of coalescence in liquids [38-40]. Thus, it is possible that coalescence is much reduced for the IL at higher pressures.

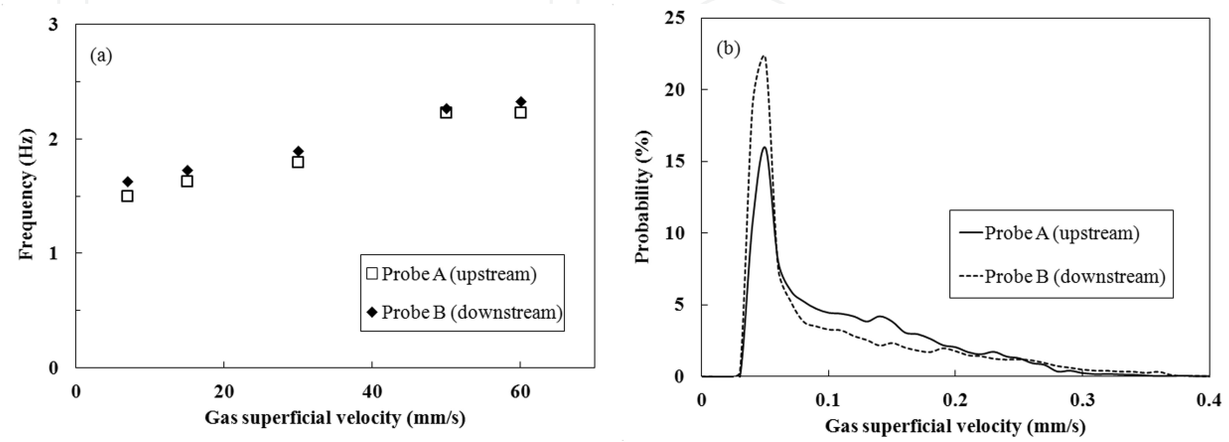

Figure 16. Effect of axial distance in $[C_2C_1Im][EtOSO_3]$: (a) frequency; (b) PDF.

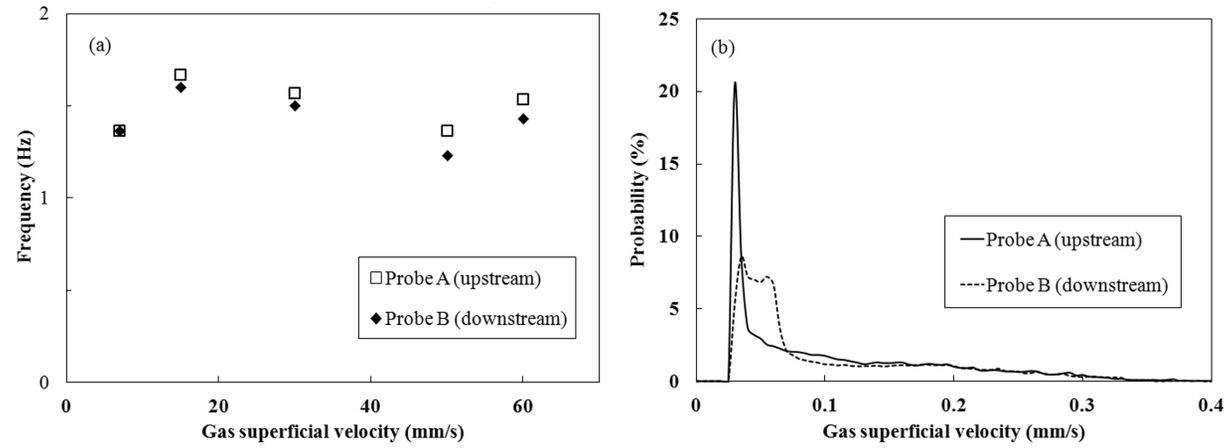

Figure 17. Effect of axial distance in glycerol + 1.3% NaCl: (a) frequency; (b) PDF.

6.3. Structure velocities

The velocities of bubbles can be determined from image analysis of high-speed videos or more objectively from cross-correlating the signals of probes placed slightly apart. For the latter, a time lag which corresponds to a peak in the cross-correlation function represents the average time required for flow structures to travel between the two probes. Since the distance between the two probes are known, the structure velocity is then easily calculated. This method of velocity measurement has been used to determine the structure velocities in $[C_2C_1Im][EtOSO_3]$. In Figure 18, the flow velocities in $[C_2C_1Im][EtOSO_3]$ at atmospheric pressure and 0.8 MPa are

shown respectively. For comparison, the equivalent data for glycerol is also presented. It can be seen that there is very good agreement between both viscous systems.

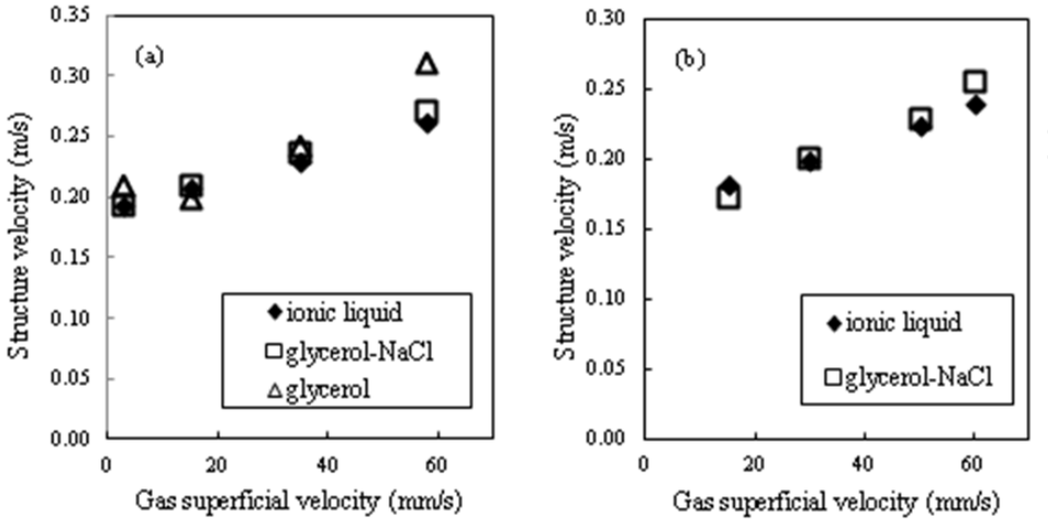

Figure 18. Effect of the liquid on the structure velocities: (a) 0.1 MPa; (b) 0.8 MPa.

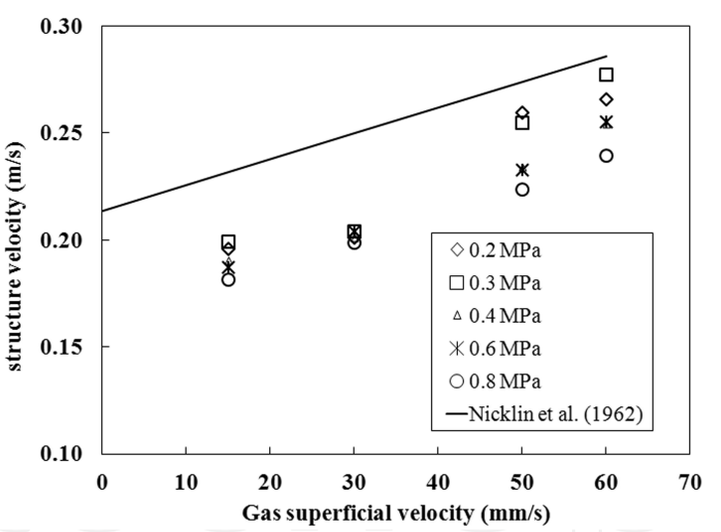

Figure 19. Effect of system pressure on structure velocities in $[C_2C_1Im][EtOSO_3]$.

The effect of increasing system pressure on the bubble rise velocities in $[C_2C_1Im][EtOSO_3]$ is illustrated in Figure 19. It is seen that in general the structure velocities decrease with increasing pressure. This is expected given the smaller bubble sizes in the system at elevated pressures. For gas-liquid flows the correlation by Nicklin et al. [41] is often used to predict the velocities of flow structures including void fraction waves and slugs. This correlation has been tested against the present IL data. It is found that the correlation predicts the correct linear trend, although with higher absolute values.

http://dx.doi.org/10.5772/51658

7. Conclusion and outlook

From the perspective of industrialization, research on the hydrodynamics of ionic liquids in bubble columns has been presented in this chapter. Despite being in its beginning stages, it is evident that this work is important for future industrial scale-up and process design. The experimental results reveal that the flow characteristics of the ionic liquid are similar to those of the other viscous media studied, both at atmospheric and elevated system pressures. Due to its high viscosity, the bubbles formed in the ionic liquid are larger compared to water which results in a significant reduction to the gas holdup. This creates smaller specific interfacial areas and less effective gas-liquid contacting. Thus to successfully achieve intimate contact between an ionic liquid and a gas stream, the viscosity of the ionic liquid is an important factor to be considered in the choice and design of industrial equipment.

Author details

Vicky Lange*, Barry J. Azzopardi and Pete Licence

*Address all correspondence to: enxls7@nottingham.ac.uk

School of Chemistry, University of Nottingham, UK

References

[1] Olivier, H. (1999). Recent Developments in the Use of Non-Aqueous Ionic Liquids for Two-Phase Catalysis. *Journal of Molecular Catalysis A, Chemical*, 146(1), 285-289.

[2] Maase, M., & Masonne, K. (2005). Bipasic Acid Scavenging Utilizing Ionic Liquids: The First Commercial Process with Ionic Liquids. Ionic Liquids IIIB: Fundamentals, Progress, Challenges, and Opportunities. *Transformations and Processes, ACS Symposium Series 902*, American Chemical Society, Washington DC, 126-132.

[3] Jork, C., Seiler, M., & Beste, Y. (2004). Influence of ionic liquids on the phase behaviour of aqueous azeotropic systems. *Journal of Chemical Engineering Data*, 49(4), 852-857.

[4] Weyershausen, B., & Lehmann, K. (2005). Industrial application of Ionic Liquids as Performance Additivies. *Green Communications*, 7(1), 15-19.

[5] Vagt, U. (2007, August 5-10). Ionic Liquids: Overview on Commercial Applications and First Toxicological Assessments. Yokohama, Japan. *In: Proceedings 2nd International Congress on Ionic Liquids (COIL)*, 125.

[6] Tempel, D., Henderson, P. B., & Brzozowski, J. (2006). Ionic Liquid based mixtures for gas storage and delivery. *US 2006/0060817 AI*.

[7] Deckwer, W. D. (1992). *Bubble Column Reactors*, New York, John Wiley and Sons Limited.

[8] Chiba, S., Idogawa, K., Maekawa, Y., Moritomi, H., Kato, N., & Chiba, T. (1989). Neutron radiographic observation of high pressure three-phase fluidization. *Fluidization VI*, Engineering Foundation, New York, 523.

[9] Krishna, R., Wilkinson, P. M., & van Dierendonck, L. L. (1991). A model for gas holdup in bubble columns incorporating the influence of gas density on flow regime transitions. *Chemical Engineering Science*, 46(10), 2491-2496.

[10] Wilkinson, P. M. (1991). Physical Aspects and scale-up of high pressure bubble columns. *PhD thesis*, University of Groningen, The Netherlands.

[11] Clark, K. N. (1990). The effect of high pressure and temperature on phase distributions in a bubble column. *Chemical Engineering Science*, 45(8), 2301-2307.

[12] Reilly, I., Scott, D. S., De Bruijn, T., & MacIntyre, D. (1994). The role of gas phase momentum in determining gas holdup and hydrodynamic flow regimes in bubble column operations. *Canadian Journal of Chemical Engineering*, 72(1), 3-12.

[13] Jiang, P., Bakshi, B. R., Zhong, H., & Fan, L. S. (1995). Analysis of flow in gas-liquid bubble columns using multi-resolution methods. *Transactions of the Institution of Chemical Engineers*, 73(6), 608-614.

[14] Lin, T. J., Reese, J., Hong, T., & Fan, L. S. (1995). Quantitative Analysis and Computation of Two-dimensional Bubble Columns. *AIChE Journal*, 42(2), 301-318.

[15] Letzel, H. M., Schouten, J. C., Krishna, R., & van den Bleek, C. M. (1999). Gas holdup and mass transfer in bubble column reactors operated at elevated pressure. *Chemical Engineering Science*, 54(13-14), 2237-2246.

[16] Kling, G. (1962). Uber die Dynamik der Blasenbildung Beim Begasen von Flussigkeiten Unter Druck. *International Journal of Heat and Mass Transfer*.

[17] Nauze, La, & Harris, I. J. (1974). Gas bubble formation at elevated system pressures. *Transactions of Institutions of Chemical Engineers*, 52, 337-348.

[18] Tsuge, H., & Hibino, S. (1980). Theoretical approach for the formation of gas bubble under the elevated system pressure G116. Japan. *Preprint of 14th Autumn Meeting of the Society of Chemical Engineers*.

[19] Schugerl, Eissa K. (1975). Holdup and backmixing investigation in co-current and counter-current bubble columns. *Chemical Engineering Science*, 30(10), 1251-1256.

[20] Wilkinson, P. M., Spek, A. P., & van Dierendonck, L. L. (1992). Design parameters estimation for scale-up of high-pressure bubble columns. *AIChE J.*, 38(4), 544-554.

[21] Kantak, M. V., Hesketh, R. P., & Kelkar, B. G. (1995). Effect of gas and liquid properties on gas phase dispersion in bubble columns. *Chemical Engineering Journal*, 59(2), 91-100.

[22] Kuncová, G., & Zahradnik, J. (1995). Gas holdup and bubble frequency in a bubble column reactor containing viscous saccharose solutions. *Chemical Engineering Process*, 34(1), 25-34.

[23] Ruzicka, M. C., Zahradnık, J., Drahoš, J., & Thomas, N. H. (2001). Homogeneous-heterogeneous regime transition in bubble columns. *Chemical Engineering Science*, 56(15), 4609-4626.

[24] Ruzicka, M. C., Drahoš, J., Fialová, M., & Thomas, N. H. (2001). Effect of bubble column dimensions on flow regime transition. *Chemical Engineering Science*, 6117-6124.

[25] Ruzicka, M. C., Drahos, J., Mena, P. C., & Teixeira, J. A. (2003). Effect of viscosity on homogeneous-heterogeneous flow regime transition in bubble columns. *Chemical Engineering Journal*, 96(1-3), 15-22.

[26] Urseanu, M. I., Guit, R. P. M., Stankiewicz, A., van Kranenberg, G., & Lommen, J. H. G. M. (2003). Influence of operating pressure on the gas hold-up on bubble columns of high viscous media. *Chemical Engineering Science*, 58(3), 697-704.

[27] Hewitt, G. F. (1978). *Measurements of Two Phase Flow Parameters*, London, Academic Press.

[28] Kumar, S. B., Moslemian, D., & Dudukovic, M. P. (1997). Gas-holdup measurements in bubble columns using computed tomography. *A.I.Ch.E. Journal*, 43(6), 1414-1425.

[29] Boyer, C., Duquenne, A. M., & Wild, G. (2002). Measuring techniques in gas-liquid and gas-liquid-solid reactors. *Chemical Engineering Science*, 57(16), 3185-3215.

[30] Fossa, M. (1998). Design and performance of a conductance probe for measuring the liquid fraction in two-phase gas-liquid flows. *Flow Measurement Instrumentation*, 9(2), 103-109.

[31] Kaji, R., & Azzopardi, B. J. (2009). Investigation of flow development of co-current gas-liquid vertical slug flow. *International Journal of Multiphase Flow*, 35(4), 335-348.

[32] Gomez, E., Gonzalez, B., Calvar, N., Tojo, E., & Domınguez, A. (2006). Physical properties of pure 1-Ethyl-3-methylimidazolium Ethyl Sulfate and its binary mixtures with ethanol and water at several temperatures. *Journal of Chemical Engineering Data*, 51(6), 2096.

[33] Clift, R., Grace, J. R., & Weber, M. E. (1978). *Bubbles, Drops, and Particles*, New York, Academic Press.

[34] Dong, H., Wang, X., Liu, L., Zhang, X., & Zhang, S. (2010). The rise and deformation of a single bubble in ionic liquids. *Chemical Engineering Science*, 65(10), 3240-3248.

[35] Riberio, C. P. (2007). On the estimation of the regime transition point in bubble columns. *Chemical Engineering Journal*, 140(1-3), 473-482.

[36] Krishna, R., Urseanu, M. I., & Dreher, A. J. (2000). Gas hold-up in bubble columns: influence of alcohol addition versus operation at elevated pressures. *Chemical Engineering and Processing*, 39(4), 371-378.

[37] Costigan, G., & Whalley, P. B. (1997). Slug flow regime identification from dynamic void fraction measurements in vertical air-water flows. *International Journal of Multiphase Flow*, 23(2), 263-282.

[38] Boyd, J. W. R., & Varley, J. (2004). Acoustic Emission Measurement of Low Velocity Plunging Jets to Monitor Bubble Size. *Chemical Engineering Journal*, 97(1), 11-25.

[39] Oolman, T. O., & Blanch, H. W. (1986). Bubble coalescence in air-sparged bioreactors. *Biotechnology Bioengineering*, 28(4), 578-584.

[40] Machon, V., Pacek, A. W., & Niwnow, A. W. (1997). Bubble sizes in electrolyte and alcohol solutions in a turbulent stirred vessel. *Chemical Engineering Research and Design*, 75(3), 339-348.

[41] Nicklin, D. J., Wilkes, J. O., & Davidson, J. F. (1962). Two-phase flow in vertical tubes. *Transactions of the Institution of Chemical Engineers*, 60, 61-68.